Study A Scanning Potential Influence on Probing Ion Trajectory in Sense of the Ion Mirror Effect.

Muayyed Jabar Zoory
Department of Physics / College of Science / AL-Mustansiriyah Univ., Iraq-Baghdad.
muayyedjz@yahoo.com

Abstract

This work is carried out to describe the behavior of an accelerated probing ion that is orientated towards a charged poly methyl-methacrylate (PMMA) sample and hence producing ion mirror images.A mathematical derivation for the path equation of this ion is based electrostatic theories aspects and on approximating of the trapped charges on the insulator as a point charge.This paper focused is to study a scanning potential influence on probing ion trajectory in sense of the ion mirror effect, in fact, this parameter (Scanning Potential) is considered from the most important parameter that control the mirror effect phenomenon. The obtained results are encouraging for using the presented procedure to simulate the ion trajectory for describing, analyzing, and adding more details to understanding ion mirror effect for further studies.

Keywords: Ion Mirror Effect (IME) phenomena, Focusing Ion Beam (FIB) and charging of insulator materials

الخلاصة

نفذ هذا العمل لوصف سلوك ايون معجل باتجاه عينة من بوليمر (PMMA) مشحونة ومن ثم انتاج صور مرآة الايون. اشتقاق معادلة المسار لهذا الايون مستندة على مفاهيم نظريات الكهربائية الساكنة وعلى تقريب الشحنة المقيدة في العازل كشحنة نقطية. ركز هذا البحث على دراسة تأثير جهد المسح على مسار الايون بمنظور تأثير مرآة الايون, في الحقيقة هذه البراميتر(جهد المسح) يعتبر من اهم البراميترات التي تسيطر على ظاهرة تأثير المرآة. ان النتائج التي تم الحصول عليها تشجع لاستعمال الاجراء المقدم ليحاكي مسار الايون من وصف, تحليل وأضافة تفاصيل اكثر لفهم تأثير مرآة آلايون للدراسات المستقبلية.

الكلمات المفتاحية: ظواهر تأثير مرآة آلايونية, تبئير الحزم الايونية و شحن المواد العازلة.

1. Introduction

Most technical dictionaries define a "dielectric" as a material of low electrical conductivity which becomes polarized under an applied electric field **(**Damamme *et al*., 1997**)**. The insulating materials like polymers and ceramics have an immense field of technological application (Ghorbel et al., 2005). Most significant case concerning the observation of dielectric substance through microscopy SEM is the charging via electron beam irradiation. Such a process leads to deviation of the incident and emitted electrons inaddition to the observation of different phenomena like a variation on the image contrast, image aberration, and magnification difference (Okai and Sohda, 2012). These influences have been discovered inside microscope SEM, known as the "charging effects" (Sikorski et al., 1968). The use of the SEM allows the charging of insulating materials to be controlled and also enable the very local charging and discharging processes to be monitored and investigated (Ghorbel et al., 2012). These effects have been observed and studied by a number of authors and can be found through the following references(Clarke and Stuart, 1970, Shaffner and Van Veld, 1971, Le Gressus *et al.*, 1991). It is important to mention, that it is observed a similar effect by using ion beam irradiation instead of electron beam inside microscope SEM/FIB for the same sample (Croccolo and Riccardi, 2008; Zoory, 2011). Great effort has been devoted to ensure that this influence does not occur. One can create a mirror electron and benefit from this effect and use it as a tool to obtain information about the model dielectric materials properties (Milani *et al.*, 2009). Recently, presented a theoretical expression is presented to describe the

scanning electron motion upon a charged sample and producing mirror image,and to present several expressions to study the most important factors that affect probing electron motion (Al-Obaidi and Khaleel, 2013).

The insulating sample is irradiated with electron or ions in SEM/FIB at high voltage. Negative or positive charge trapped in the insulator during the injection produces an excess charge which is spatially trapped within the sample generating distortions in the electrons or ions paths. To get a mirror effect, then later process of the sample rasters with electron or ion beam of energy smaller than the repulsive potential energy of the sample surface.

The probing ion which has a small kinetic energy which will be reflected in the back parts of the FIB chamber due to repulsion force between the trapped ions on the surface and the probing ion.This effect depends on the probing ion direction and beam parameters. The reflected backward ions will bombard the FIB chamber inner walls and cause to release new secondary electrons that their detection leads to image the insider chamber space, which characteristics depend on the chamber materials and primary ion energy (Scanning Potential)., see Fig. 1. The secondary electrons are then detected by the Everhard-Tornley Detector (ETD) within the chamber to form the ion mirror image of the (FIB) chamber itself.

Fig. 1 shows a scheme of the Ion Mirror Effect (IME), it is clear that most parameters influencing the production of the ion mirror image (IMI) is the scanning potential, so the present work studies the effect of this parameter on the probing ion path by building a mathematical model for the ion path.

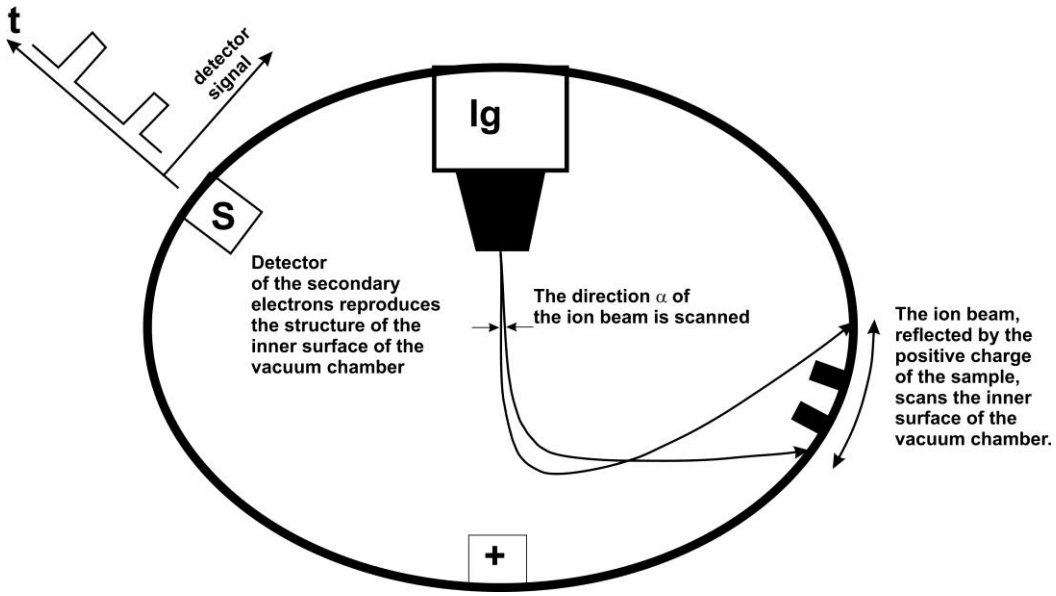

Fig. 1. A schematic diagram revealing the Ion Mirror Effect (IME) phenomena.

2. Theoretical Aspects

The approximation of the point charge distribution is used to calculate the trapped charge (Q_i), that accumulated on the sample surface in the FIB, being a point charge which is stationary at an arbitrary point likes C. Fig.2 shows a probing ion

(e^+) of an initial velocity ($v_\circ$) approaching from trapped charge along the line AB and angle (α(degree)) relative to the line AC.

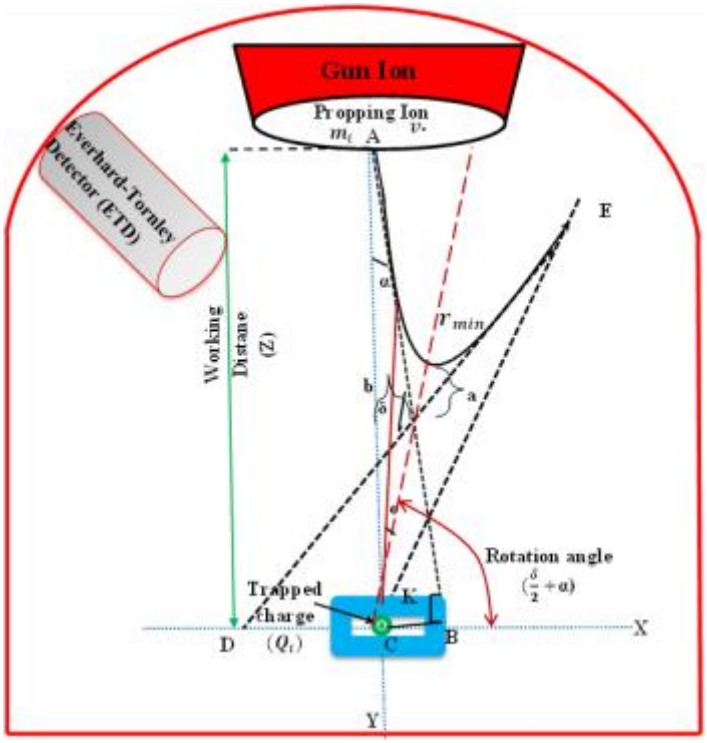

Fig. 2. A drawing sketch for the probing Ion path inside an FIB chamber in sense of Ion Mirror Effect (IME) which illustrated the scattering angle computation and the derivation of the ion path equation.

The relation between trapped charge (Q_i) with a relative dielectric constant (ε_r), is equal to the charge placed in free space $2Q_i/(\varepsilon_r+1)$ (Jackson, 1999). Thus, the repulsion force between the probing ion in FIB and the trapped ions embedded in a dielectric sample inside chamber FIB takes the form(Jackson, 1999)

$$F(z) = \frac{A_\infty e^+ Q_i}{Z^2} \quad (1)$$

In which A_∞ is a constant defined by $A_\infty = 1/2\pi\varepsilon_\circ(\varepsilon_r + 1)$, $\varepsilon_\circ$ is permittivity of free space and Z is the distance of the probing ion from the trapped charge (Q_i). We will start from Newton's second law in radial and transverse direction can be appropriate to study the path probing ion trajectory in asense of ion mirror effects.

$$m_i\left[\frac{d^2z}{dt^2} - z\left(\frac{d\theta}{dt}\right)^2\right] = \frac{A_\infty e^+ Q_i}{Z^2} \quad (2)$$

$$m_i\left[\frac{d^2z}{dt^2} + 2\left(\frac{dz}{dt}\right)\left(\frac{d\theta}{dt}\right)\right] = 0 \quad (3)$$

In which m_i is the probing ion rest mass. From the last equation, we get

$$m_i Z^2 \frac{d\theta}{dt} = \text{Constant} = L \quad (4)$$

Where (L) is angular momentum which can be defined as

$$L = Zm_i v_\circ \sin\alpha = m_i v_\circ K \quad (5)$$

Where (k) represents the perpendicular distance between the tangent to the path of the probing ion AB and the trapped charge , Fig. 2. shows and $v_\circ$ is the initial velocity takes the form

$$v_\circ = \sqrt{\frac{2e^+V_{sc}}{m_i}} \quad (6)$$

The use of chain rule with new variable $(s = \frac{1}{z})$ may lead to convert Eq. (2) to the equation that are not dependent on the time, because the imaging processes occur in ultra-short time, as following;

$$\frac{d^2}{d^2\theta}\left[s + \frac{A_\infty Q_i}{2V_{sc}K^2}\right] + \left[s + \frac{A_\infty Q_i}{2V_{sc}K^2}\right] = 0 \quad (7)$$

The solution is

$$s = \frac{1}{Z} = \frac{A_\infty Q_i Z^2}{2V_{sc}K^2}(\mu\cos\theta - 1) \quad (8)$$

In which $\mu = \frac{2AV_{sc}K^2}{A_\infty Q_i}$, where A is constant to be determined according to initial conditions. So the probing ion path can be determined once θ and μ are known. By the differentiation of both sides for Eq.(8), we get

$$\frac{dZ}{d\theta} = \frac{A_\infty Q_i Z^2}{2V_{sc}K^2}\mu\sin(\theta) \quad (9)$$

It is seen that, Eq. (8) represents a form of equations of a conic section in polar coordinate where μ is the eccentricity of this conic section. However, an equation to determine the eccentricity of the probing ion path with the aid of the principle of conservation of energy can be written as:

$$e^+V_{sc} = \frac{1}{2}m_i v^2 + \frac{A_\infty e^+ Q_i}{Z} \quad (10)$$

We will use the chain rule to the resolving the velocity of the probing ion as follows:

$$v^2 = \left(\frac{d\theta}{dt}\right)\left[Z^2 + \left(\frac{dZ}{d\theta}\right)^2\right] \quad (11)$$

Substituting Eqs. (8), (4) and (9) in Eq. (11), we get

$$v^2 = \frac{A_\infty{}^2 e^+ Q_i{}^2}{2m_i V_{sc}K^2}(1 + \mu^2 - 2\mu\cos(\theta)) \quad (12)$$

Substituting Eq. (12), in Eq. (10) with the aid of that of Z expressed in Eq. (8), we get

$$\mu = \left(\frac{A_\infty{}^2 Q_i{}^2 + 2V_{sc}{}^2 K^2}{A_\infty{}^2 Q_i{}^2}\right)^{-1/2} \quad (13)$$

Now, by substituting Eq. (13) in Eq. (8), we get

$$Z(\theta) = \frac{2V_{sc}K^2}{A_{\infty}Q_i\left[\left(1+\frac{4V_{sc}^2K^2}{A_{\infty}^2Q_i^2}\right)^{1/2}\right](\cos\theta-1)} \quad (14)$$

This equation can be used to simulate the trajectory of probing ion, as a function of zimuthal coordinate θ, during its travel from the column diaphragm till the FIB chamber. From Fig.2 , we yield

$$\left(\frac{\pi}{2}-\frac{\delta}{2}-\alpha\right) \leq \theta \leq -\left(\frac{\pi}{2}-\frac{\delta}{2}-\alpha\right) \quad (15)$$

Where δ is the scattering angle (angle between the asymptotes of the probing ion path before and after scattering) and α is the incident angle. Furthermore, from Fig.2 ,we get

$$\tan\left(\frac{\pi-\delta}{2}\right) = \frac{b}{a} = \cot\left(\frac{\delta}{2}\right) \quad (16)$$

In fact, the eccentricity of conic section equations theory, can be expressed as follows (Anton et al., 2002)

$$\frac{b}{a} = (\mu^2-1)^{1/2} \quad (17)$$

Where the numbers a and b are called the semi major axis and the semi minor axis respectively.

From Eq. (16) and Eq. (17), we obtain to

$$\cot\delta = \frac{2}{(\mu^2-1)^{1/2}} \; or \; \delta = 2\cot^{-1}(\mu^2-1)^{1/2} \quad (18)$$

Thus, from Eq. (14) it is possible to simulate the path of the probing ion where the incident angle (α), trapped charge (Qi), relative dielectric constant (ε_r) and scanning potential (Vsc) are known.

Calculations of the minimum approach distance (Z_{min}) refers to the shorter distance from the trapped charge. It has an importance because it gives indications about the reflection point of probing ion path (see Fig.. 2). Therefore, from Eqs. (14) and (15) one can observe the distance of minimum approach in the following formula ;

$$Z_{min} = \frac{2V_{sc}K^2}{A_{\infty}Q_i\left[\left(1+\frac{4V_{sc}^2K^2}{A_{\infty}^2Q_i^2}\right)^{1/2}\right]-1} \quad (19)$$

The axial and vertical Cartesian coordinates of the point of reflection are given by the following two expressions respectively:

$$x_{min} = \frac{2V_{sc}K^2}{A_{\infty}Q_i\left[\left(1+\frac{4V_{sc}^2K^2}{A_{\infty}^2Q_i^2}\right)^{1/2}\right]-1}\cos\left(\frac{\delta}{2}+\alpha\right) \quad (20)$$

$$y_{min} = \frac{2V_{sc}K^2}{A_{\infty}Q_i\left[\left(1+\frac{4V_{sc}{}^2K^2}{A_{\infty}{}^2Q_i{}^2}\right)^{1/2}\right]-1}\sin\left(\frac{\delta}{2}+\alpha\right) \quad (21)$$

It is well known that the equipotential surfaces due to a point charge that have a spherical shape or equivalently the Gaussian surface for a point charge are spherical surfaces. Thus, the electric potential in a SEM\FIB chamber vacuum can be expressed as follows (Al-Obaidi and Khaleel, 2013);

$$V_s(z) = \frac{2Q_i}{4\pi\epsilon_\circ(\epsilon_r+1)Z} \quad (22)$$

Where $= \sqrt{x_i^2 + y_i^2}$, we yield

$$V_s(x_i, y_i) = \frac{2Q_i}{4\pi\epsilon_\circ(\epsilon_r+1)\sqrt{x_i^2+y_i^2}} \quad (23)$$

Along the optical y-axis that means $x_i = 0$ the Eq. (23) converted to the following form;

$$V_s(y_\circ) = \frac{2Q_i}{4\pi\epsilon_\circ(\epsilon_r+1)y_\circ} \quad (24)$$

The left hand side of Eq. (23) must be replaced by $V_s(y_\circ)$ to find all of the points (x_i, y_i) that has a same potential $V_s(y_\circ)$. Then Eq. (23) becomes;

$$x_i = \mp\sqrt{\left(\frac{2Q_i}{4\pi\epsilon_\circ(\epsilon_r+1)V_s(y_\circ)}\right)^2 - y_i^2} \quad (25)$$

Eq. (25) can be used to calculate the equipotential surface, surrounded the trapped charge on the sample, that has the value $V_s(y_\circ)$.

3. Results and discussion

The kinetic energy for probing ion depends on potential which is used to produce an ion mirror image (IMI). Thus, one may directly realize that scanning potential had a great influence on probing ion trajectory in sense of ion mirror effects.

Some of the results presented in the reference (Zoory, 2014)are adopted here to investigate the scanning potential influence on ion mirror image (IMI) formation. Fig. 3a shows several ion mirror images which are imported from the reference (Zoory, 2014). Actually a poly-methyl-methacrylate (PMMA) is irradiated with an ion beam of a potential Vi=30kV for five minutes over an area of radius ≈ 0.457mm. The temperature, pressure, working distance and tilt angle are maintained fixed for all of the experiments of this work at the following values; room temperature, 2.0×10^{-5} Pa, 30mm and 52° respectively, and so the PMMAsample acquired a trapped charge off amount (Qt=508pC). Thereafter, these images are received at different potentials as indicated in this figure. The correspondence simulators for the probing ion paths belong to these images are plotted in figure 3b.

However, several remarks can be read from the simulation graphs, the scattering angle δ for paths belong to the same image decreases as the impact parameter K (strictly speaking α) increases. In fact, since the coulomb force between the probing ion and the trapped charges has an inverse proportional with the quadratic of separated distance. Therefore, as α increased for such a path the radial distance ($Z(\theta)$) between the ion and trapped charge gets rise increases, and hence the interaction strength becomes weaker and vice versa. In other word, one may say that, the outer probing ion, in a scanning beam, will scan distant regions of the chamber's ceiling, while the inner ones hit the nearby regions.

The Fig.3 reveals more details of the ceiling chamber in the image of V_{sc}=6 kV in comparison with its counterpart of V_{sc}=8, 10 and 12 kV. Furthermore, opportunities for the probing ions to reach the sample regions increase as the scanning potential (V_{sc}) increased. According to the last discussed result, that is why some parts of the sample's regions which are not irradiated (free of charges) appear in the third image and the fourth image (Vsc=10 kV and Vsc=12 kV), while it does not exist in the first (Vsc=6 kV) and second images (Vsc=8 kV). For more carification, the inset figures have been added to Tables (1, 2, 3 and 4), where (x_{min},y_{min}) is a point of shorter distance from the trapped charge before totally reflected, while (x_{max},y_{max}) is a point of maximum distance from the trapped charge after totally reflected inside FIB.

It is seen that probing ion reflected at a higher distance from the sample as the scanning potential increases and vice versa. Indeed, it is an expected result, since increases of scanning Potential lead to increasing the repulsion force that they exert on probing ion. Thus, such an ion will be back scattered at a point away from the sample surface whenever scanning Potential increases. So, as long as images of mirror effect are received at higher scanning potential, they will be characterized with a wide field of view. In other words, an FIB user has an opportunity to view wider areas of the chamber, by means of mirror effect images, whenever a higher scanning potential is used to capture these image

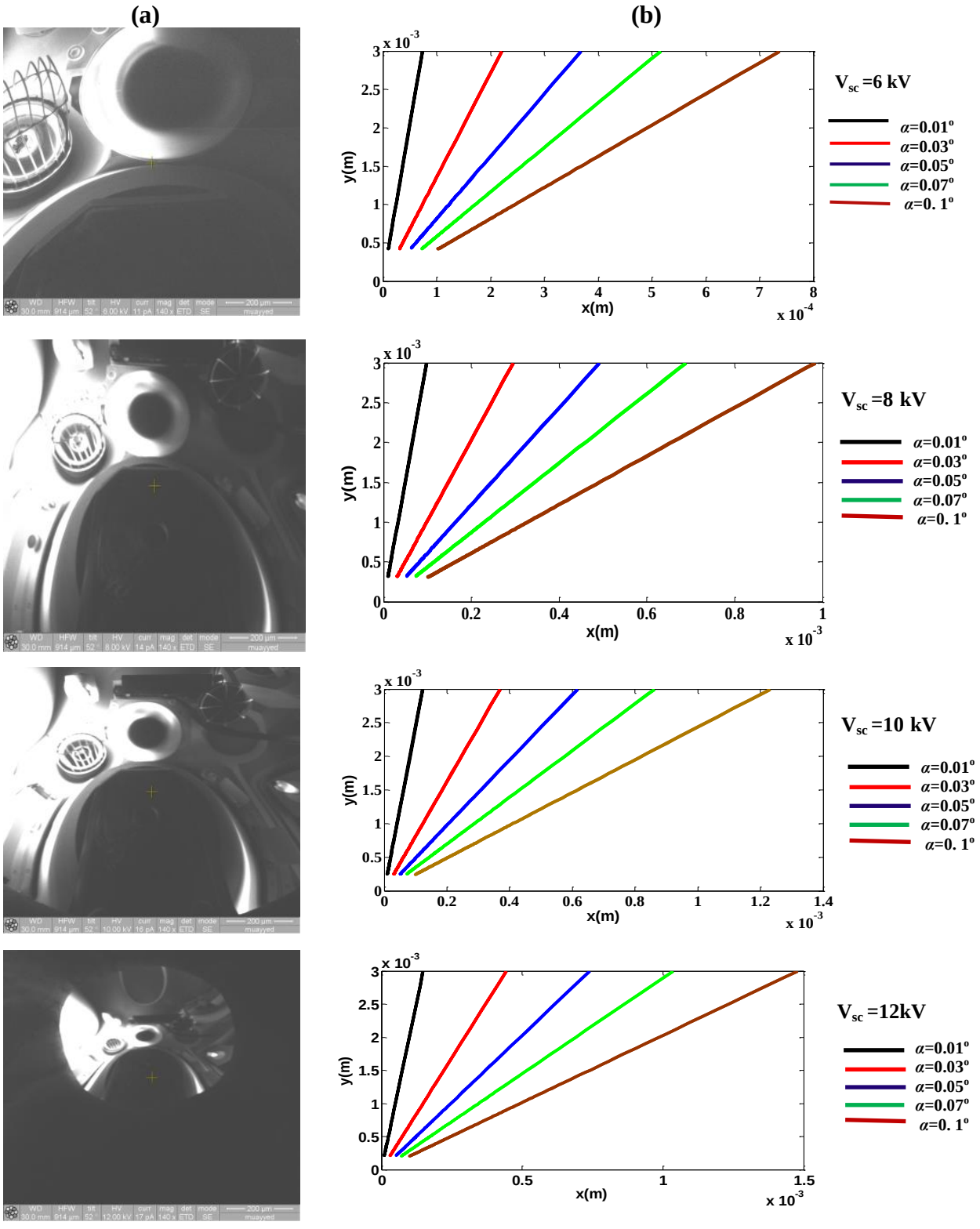

Figure 3: (a) IMI recorded at different scanning potential with V_i=30kV, (Zoory, 2014)(b) their corresponding simulated ion paths according to the present work.

In order to strengthen the argument above, paths of similar incident angle (α=0.01^o) but different scanning potential, have been plotted in Fig. 4. So when the energy of incident ions increased, they will be reflected toward wider regions in the chamber and hence more information can be collected.

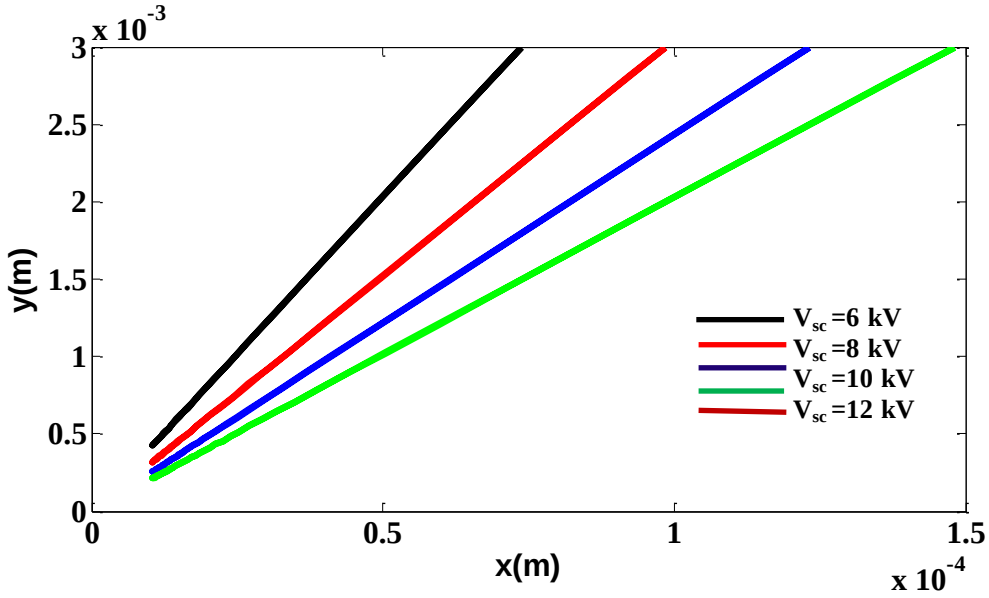

Figure 4: Different probing ion paths of a same incident angle reflect to the different points.

Table 1: Variation of the values (x_{min}, y_{min}) and (x_{max}, y_{max}) with scanning potential (V_{sc}=6KV) for different incident angle (α).

α (degree)	x_{min}(mm)	y_{min}(mm)	x_{max}(mm)	y_{max}(mm)
0.01^o	0.0104	0.4229	0.7339	0.0301
0.03^o	0.03115	0.4224	2.214	0.03002
0.05^o	0.05179	0.4214	3.673	0.02998
0.07^o	0.07225	0.4199	5.105	0.02976
0. 1^o	0.1025	0.4169	7.185	0.02924

Table 2: Variation of the values (x_{min}, y_{min}) and (x_{max}, y_{max}) with scanning potential (V_{sc}=8 KV) for different incident angle (α).

α (degree)	x_{min}(mm)	y_{min}(mm)	x_{max}(mm)	y_{max}(mm)
0.01^o	0.01041	0.3172	0.9872	0.03006
0.03^o	0.0315	0.3151	2.9490	0.02993
0.05^o	0.05174	0.3151	4.8730	0.02968
0.07^o	0.07198	0.3132	6.7370	0.02932
0. 1^o	0.1015	0.3094	9.3800	0.02858

Table 3: Variation of the values (x_{min}, y_{min}) and (x_{max}, y_{max}) with scanning potential (V_{sc}=10KV) for different incident angle (α).

α (degree)	x_{min}(mm)	y_{min}(mm)	x_{max}(mm)	y_{max}(mm)
0.01^o	0.01043	0.2114	1.4810	0.03002
0.03^o	0.03116	0.2528	3.6780	0.02984
0.05^o	0.05160	0.2512	6.0490	0.02945
0.07^o	0.07156	0.2489	8.3080	0.02889
0. 1^o	0.10030	0.2444	11.4200	0.02781

Table 4: Variation of the values (x_{min}, y_{min}) and (x_{max}, y_{max}) with scanning potential (V_{sc}=12kV) for different incident angle (α).

α (degree)	x_{min}(mm)	y_{min}(mm)	x_{max}(mm)	y_{max}(mm)
0.01°	0.01043	0.2114	1.4810	0.03002
0.03°	0.03114	0.2103	4.4010	0.02973
0.05°	0.05141	0.2084	7.1970	0.02918
0.07°	0.07103	0.2057	9.8080	0.02841
0. 1°	0.09893	0.2007	13.2900	0.02696

Another observation can be seen in Fig. 4, that is, the probing ion approaches nearer the sample as its own scanning potential increases. Equivalently one may say that, the point of inflection in the path occur far away from the FIB column as V_{sc} increases. Accordingy the images presented in Fig. 3a appear to be moving away from the column aperture as scanning potential increases. Hence it is concluded that when the potential is further raised, the ion mirror effect image will disappear as the ion will be stopped at a minimum distance from the surface (i.e. The maximum accelerating potential (V_{sc}^{max}) In which a mirror effect will happen when the probing ion will be stopped at a minimum distance from the sample) see Fig. 5.

From Eq. (23) the maximum accelerating potential (V_{sc}^{max})can be calculated when the probing ion will be stopped at a minimum distance from the surface. Actually, it is clear from Table 5, when the value of the incidence angle equals 0.01 the value of $V_{sc}^{max}(x_{min},y_{min})(KV)$ approaches 20 kV. In fact, this means that the point charge approximation is limited with small incident angles.

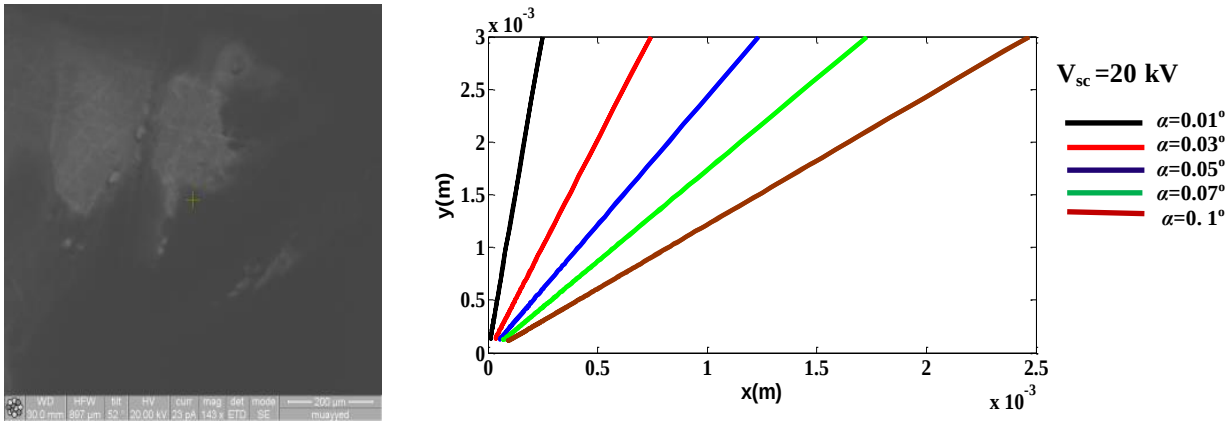

(a) **(b)**

Figure 5: (a) ion mirror effect imported from reference (Zoory, 2014) (b) their corresponding simulated ion paths according to the present work.

Table 5: Variation of the values (x_{min}, y_{min}) and (x_{max}, with y_{max}) scanning potential (V_{sc}=20kV) for different incident angle (α).

α (degree)	x_{min}(mm)	y_{min}(mm)	$V_{sc}^{max}(x_{min},y_{min})(KV)$	x_{max}(mm)	y_{max}(mm)
0.01°	0.01043	0.1267	19.972	2.4650	0.02993
0.03°	0.03089	0.1250	19.719	7.2030	0.02916
0.05°	0.05027	0.1221	19.228	11.4300	0.02777
0.07°	0.06824	0.1185	18.567	14.9900	0.02602
0. 1°	0.09255	0.1125	17.429	19.0908	0.02320

Fig. 6 shows the vertical coordinates of the inflection points as a function of the horizontal one for paths of different inclination angle. It is seen that, the vertical coordinate for inflection points decreases, while its counterpart for the horizontal one increases as α increases. But the decreases in y-coordinate is less significant compared with that in x-coordinate. Such aresult may be interpreted as that the transverse component of the repulsive force that the probing ions suffer from being gradually increased as the path deviation increases. So, these ions are forced to deflect away from the center of trapped charges, located at the origin, in the transverse direction faster than the vertical one.

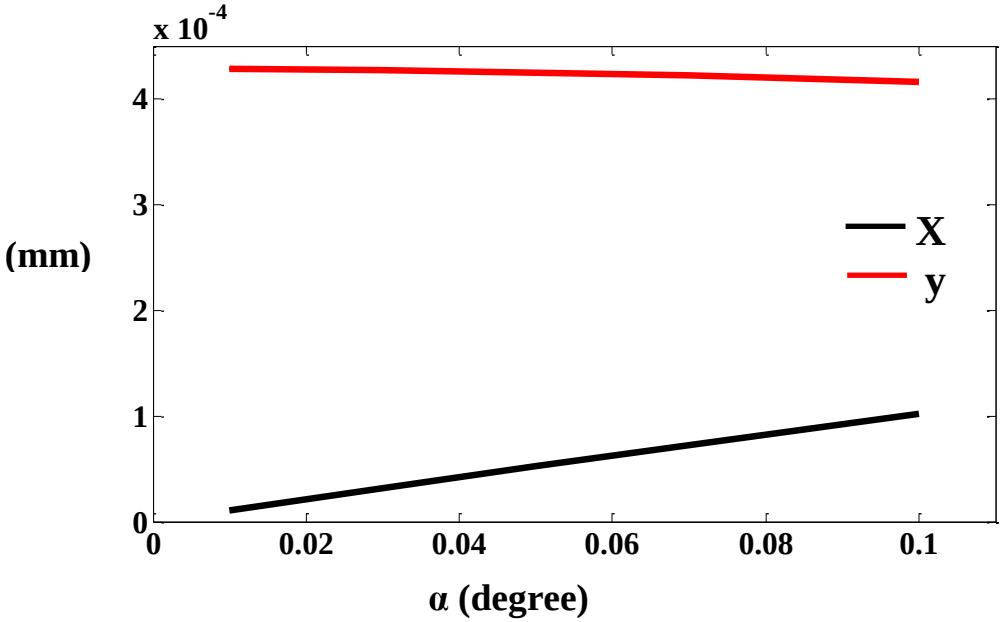

Figure 6: The Variation of the horizontal and vertical coordinates of reflection points with different incident angle for scanning potential 6kV.

Actually, what have been mentioned in the last paragraph can be summarized by means of Fig.7. It can be seen that the variation interval for x is large compared with that of y. It is well known that the equipotential surfaces belong to a charge point have equivalently the Gaussian surface appropriate, or a spherical shape for charge point is a spherical surface. While the curve plotted in the Fig.7, in general, it can be considered as a part of ellipse profile rather than spherical one. Defiantly, the reason is that the assumption of the trapped charge to be a charge point, in the sense of the framework of the present work is just an approximation. However, Fig.7 may seem to be the surfaces that surround the trapped charge located at a point. Thus, such a curve could be an equipotential surface deduced by charges accumulated at a point.

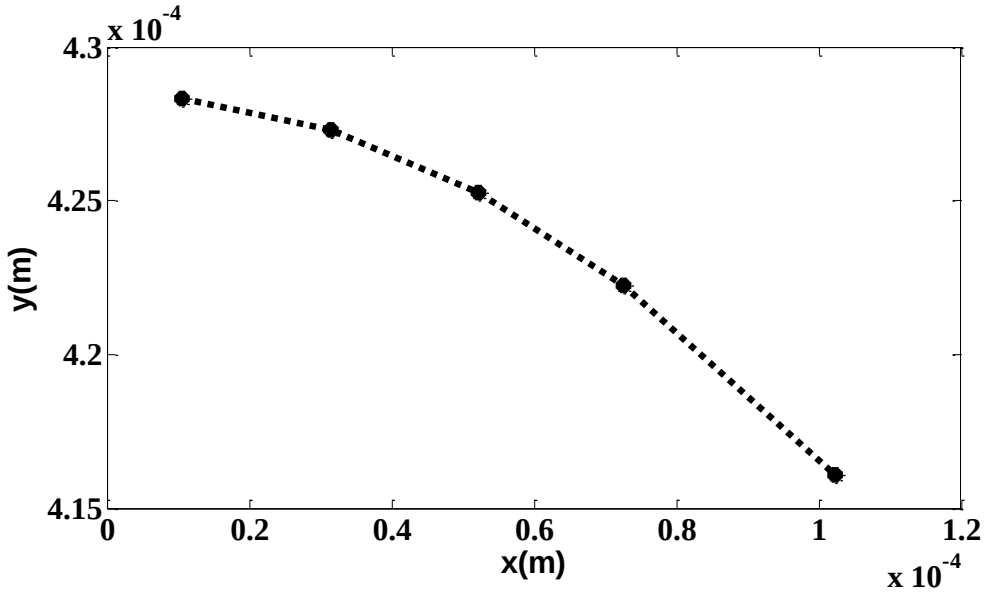

Figure 7: The variation of the horizontal coordinates of reflected points as a function of vertical, one for paths of different incident angle.

For more clarification, Fig. 8 shows the probing ion paths for the Vi=30KV and trapped charge (508pC), together with the equipotential surfaces that are computed by means of Eq. 25. The figure reveals that all of the plotted paths reflected at points lying at the equipotential of potential value 6KV. However, such an issue needs further investigation, hence we will insert Fig.3b at v=6KV to the Fig. 7 we get Fig. 9. Actually, this result agrees with the result in Fig. 8 which represents equipotential surfaces.

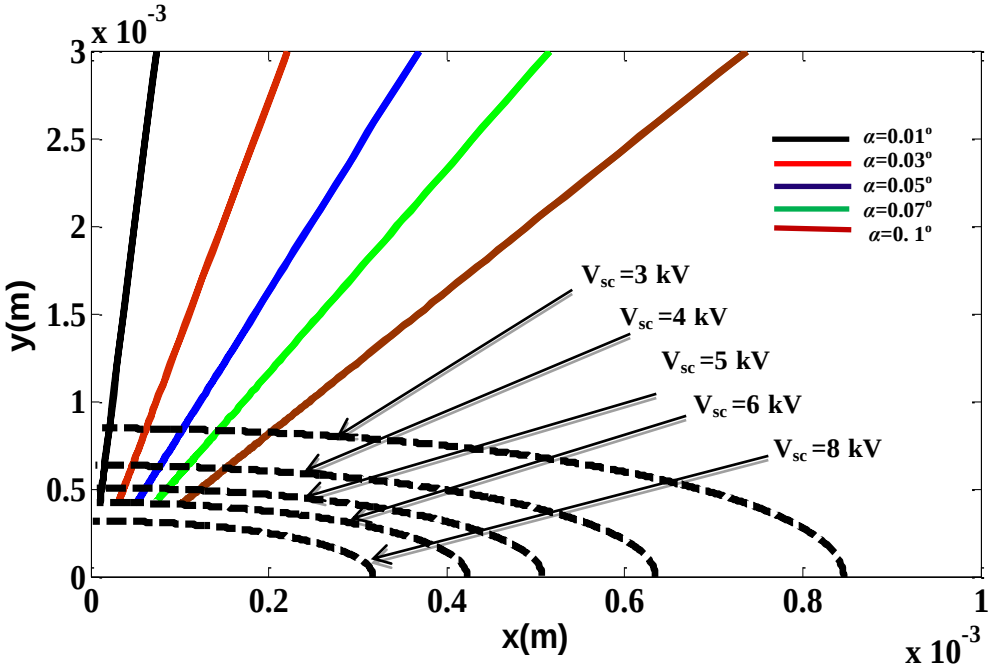

Figure 8: Probing ion path and equipotential surface at V_{sc}=6kV.

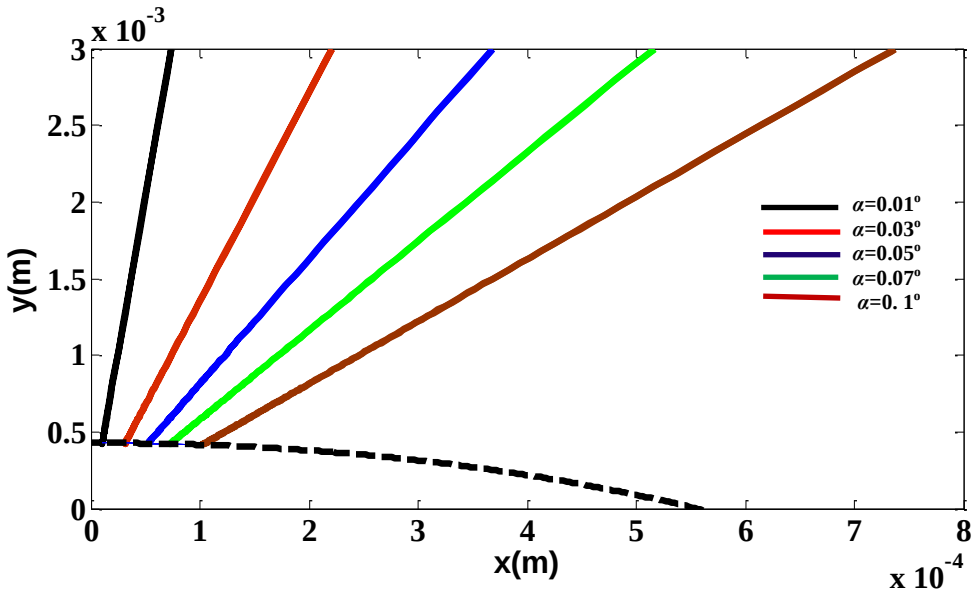

Figure 9: the figure 3b at v=6KV insert to the figure 7

The variations of the scattering angle as a function of the incident angle, at different scanning potential, have been plotted in Fig.10. Besides the usual variation of the scattering angle with the incident one, one may recognize that, whenever the Vsc of a high value is used, the scattering angle of the path of a similar incident angle will decrease. Interpretation for this result is that, the increases of Vsc lead to increase in velocity of the probing ion and so its kinetic energy. Consequently, the faster ion had less deflection compared with the slow one, and hence the scattering angle decreases.

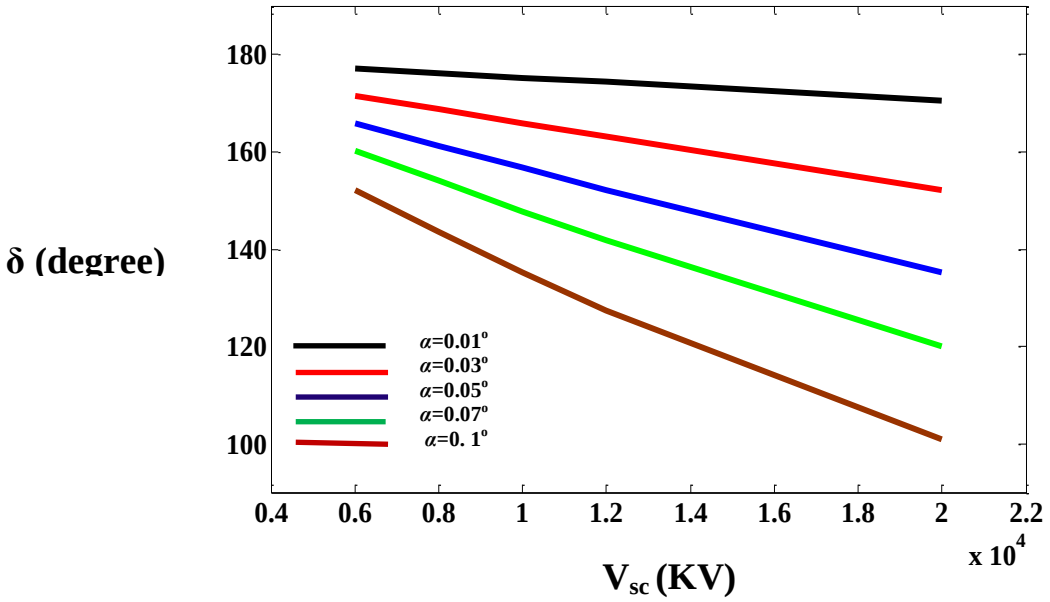

Figure 10: Variation of scattering angle (δ (degree)) with the scanning potential (V_{sc} (KV)) for paths of different incident angle.

In order to give the last argument, evidence, the scattering angles versus the inclination angle have been plotted in Fig.11, for different scanning potential. Typically, the scattering angle decreases whenever the path inclination increased. In addition, this behavior is clearer as the used scanning potential increased.

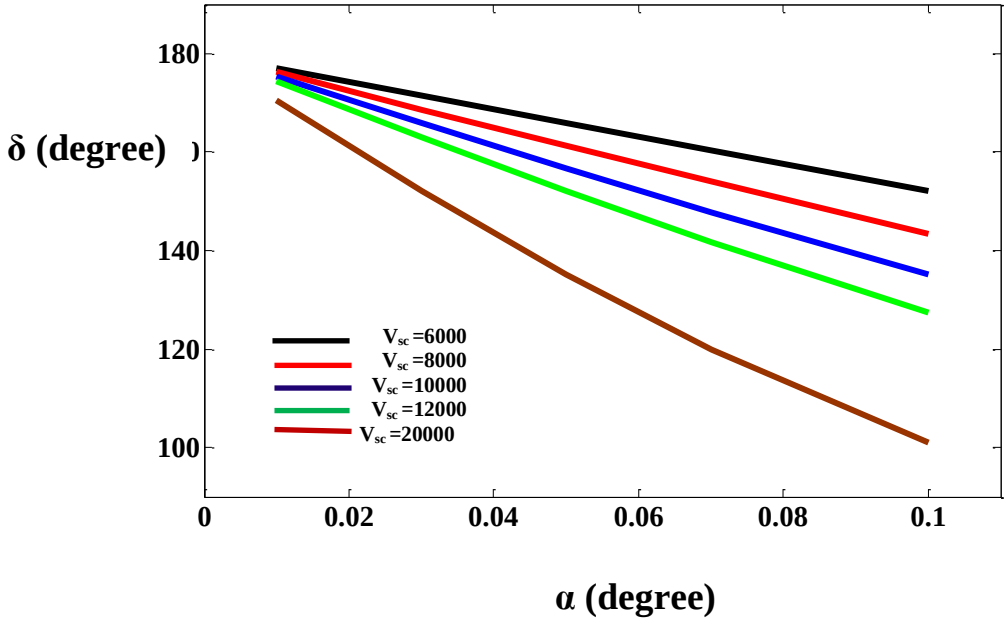

Figure 11: Variation of scattering angle with the incident one at different scanning potential.

Conclusions

The Focus Ion Beam (FIB) apparatus is an important consequence for analyzing insulator materials. The results have shown that the assumption of the point charge distribution which has been adopted in this work reveal an excellent interpretation of the ion mirror images. Additionally, it is often possible to locate the reflected-back probing ions by means the mathematics presented in this investigation. Consequently, one may easily recognize what path, that probing ions will follow, can enter column diaphragm or will reach detectors.

Additional conclusion remarks can be recorded for this study, for instance the reflected points (a minimum distance from the surface) representing equipotential surfaces, from the reflected points can deduce the maximum accelerating potential (V_{sc}^{max}) for the different incidence angle, moreover, excellent accuracy in calculating the number of ions (or charges) can be accumulated at a surface of an insulator at the different work conditions.

Reference

AL-OBAIDI, H. N. & KHALEEL, I. H. 2013. Computational investigation of electron path inside SEM chamber in mirror effect phenomenon. *Micron,* 51**,** 13-20.

ANTON, H., BIVENS, I. & DAVIS, S. 2002. *Calculus 7th ed.,* John Wiley & Sons, Inc., USA.,

CLARKE, D. & STUART, P. 1970. An anomalous contrast effect in the scanning electron microscope. *Journal of Physics E: Scientific Instruments,* 3**,** 705.

CROCCOLO, F. & RICCARDI, C. 2008. Observation of the ion-mirror effect during microscopy of insulating materials. *Journal of microscopy,* 229**,** 39-43.

DAMAMME, G., LE GRESSUS, C. & DE REGGI, A. 1997. Space charge characterization for the 21th century. *Dielectrics and Electrical Insulation, IEEE Transactions on,* 4**,** 558-584.

GHORBEL, N., KALLEL, A. & DAMAMME, G. 2012. Modeling electric charge distribution on insulator under electron bombardment: Case of rectangular surface implantation. *AIP Advances,* 2**,** 012190.

GHORBEL, N., KALLEL, A., DAMMAME, G., RENOUD, R. & FAKHFAKH, Z. Space charge in irradiated insulators: mirror method. Electrets, 2005. ISE-12. 2005 12th International Symposium on, 2005. IEEE, 235-238.

JACKSON, J. D. 1999. *Classical Electrodynamics,* John Wiley, New York.

LE GRESSUS, C., VALIN, F., HENRIOT, M., GAUTIER, M., DURAUD, J., SUDARSHAN, T., BOMMAKANTI, R. & BLAISE, G. 1991. Flashover in wide-band-gap high-purity insulators: Methodology and mechanisms. *Journal of applied physics,* 69**,** 6325-6333.

MILANI, M., BIGONI, D. & SAVOIA, C. 2009. Electron mirroring: control of electron transport and understanding of physical processes from SEM images. *Proceedings of ITP2009. Interdisciplinary Transport Phenomena VI, Volterra, Italy,* 6.

OKAI, N. & SOHDA, Y. 2012. Study on image drift induced by charging during observation by scanning electron microscope. *Japanese Journal of Applied Physics,* 51**,** 06FB11.

SHAFFNER, T. & VAN VELD, R. 1971. 'Charging'effects in the scanning electron microscope. *Journal of Physics E: Scientific Instruments,* 4**,** 633.

SIKORSKI, J., MOSS, J., NEWMAN, P. & BUCKLEY, T. 1968. A new preparation technique for examination of polymers in the scanning electron microscope. *Journal of Physics E: Scientific Instruments,* 1**,** 29.

ZOORY, M. J. 2011. *Mirror Effect Investigation For Focused Ion Beams* Ph.D.Thesis, University of Al-Mustansiriyah.

ZOORY, M. J. 2014. New way to overcome on the mirror effect for imaging the surface of insulator. *IOSR Journal of Applied Physics,* 6**,** 12-20.